Nonlinear Dyn (2010) 59: 545–558
DOI 10.1007/s11071-009-9561-5

ORIGINAL PAPER

Potential benefits of a non-linear stiffness in an energy harvesting device

R. Ramlan · M.J. Brennan · B.R. Mace · I. Kovacic

Received: 14 July 2008 / Accepted: 3 July 2009 / Published online: 28 July 2009

Abstract The benefits of using a non-linear stiffness in an energy harvesting device comprising a mass–spring–damper system are investigated. Analysis based on the principle of conservation of energy reveals a fundamental limit of the effectiveness of any non-linear device over a *tuned* linear device for such an application. Two types of non-linear stiffness are considered. The first system has a non-linear bi-stable snap-through mechanism. This mechanism has the effect of steepening the displacement response of the mass as a function of time, resulting in a higher velocity for a given input excitation. Numerical results show that more power is harvested by the mechanism if the excitation frequency is much less than the natural frequency. The other non-linear system studied has a hardening spring, which has the effect of shifting the resonance frequency. Numerical and analytical studies show that the device with a hardening spring has a larger bandwidth over which the power can be harvested due to the shift in the resonance frequency.

R. Ramlan (✉) · M.J. Brennan · B.R. Mace
Institute of Sound and Vibration Research, University of Southampton, Southampton SO17 1BJ, UK
e-mail: rr@isvr.soton.ac.uk

I. Kovacic
Department of Mechanics, Faculty of Technical Sciences, University of Novi Sad, 21121 Novi Sad, Serbia

Keywords Energy harvesting · Snap-through · Hardening · Negative stiffness

1 Introduction

Vibration-based energy harvesting devices have received much attention over the past few years because of the need to power wireless devices in remote or hostile environments. To date, a resonant linear generator has been the most common type of generator used in harvesting energy. Simple tuning and modelling methods described in [1] make it a more favourable solution theoretically, if not practically. The model for such a device provides valuable insight into the main transduction mechanisms, such as electromagnetic, piezoelectric and electrostatic [2], used for this application. However, good performance of the generator is limited to a narrow frequency band when the device is optimally tuned so that its natural frequency coincides with the excitation frequency. The performance of the resonant generator drops off rapidly if mistuned. Sari et al. [3] have developed a wide-band micro power generator in order to overcome this limitation by employing a series of cantilevers with various lengths and resonance frequencies, which is suitable for high frequency applications (3.5–4.5 kHz). In addition, the power harvested by a resonant device is proportional to the cube of the excitation frequency [1], which then limits the performance of the resonant generator even more at low frequencies.

The low frequency applications of interest in the work presented here are body-worn devices such as mobile phones, ipods, digital cameras and a cochlear implant. The body-worn device is improving in terms of technology and is becoming smaller in size. From the energy harvesting point of view, this will limit the distance that the seismic mass in the generator can travel even more. This means that system damping has to be increased to limit the travel of the mass [4]. However, an increase in system damping considerably reduces the power harvested by a resonant generator operating at resonance. Another factor is that a linear device must be designed to have a low natural frequency, which means that a large mass and a soft spring element are required. For body-worn applications, a soft spring may be acceptable but a larger mass, which adds extra weight to a small device, is not. In addition, having a large mass supported on a soft spring may result in some non-linearity due to the large extension of the spring. Thus, to overcome this limitation, other types of generator need to be investigated, including non-resonant generators, which have comparable or better performance than a resonant generator. Kulah and Najafi [5] developed a generator which converts low frequency ambient vibrations to a much higher frequency through an electromechanical frequency up-converter using a magnet that provides efficient energy conversion even for low ambient frequencies. Another frequency up-conversion mechanism has been studied by Lee et al. [6] employing piezoelectric technology. Mitcheson et al. [7] discussed three architectures for energy harvesting devices. One of the architectures described is a new non-resonant non-linear mechanism termed a Coulomb-force parametric generator (CFPG). This mechanism is useful when the allowable mass frame displacement is small compared to the vibration source amplitude and for frequencies well below the resonant frequency of the resonant generator. However the limit of the ratio of the power harvested using the CFPG mechanism to that using a resonant mechanism was found to be $4\beta/\pi$ where $0 < \beta < 1$. This CFPG mechanism was then used in [8] along with other mechanisms described in [7] to study the amount of energy that can be harvested from human walking motion by using measured data from various parts on the body. A recent advance in this field has been to incorporate a non-linear compliance, typically a hardening system, to increase the bandwidth of the system [9] by shifting the resonance frequency. However, to the authors' knowledge, no analytical solution has been presented for the bandwidth of such a device.

This paper describes two non-linear mechanisms for energy harvesting devices. They consist of two types of non-linear spring connected to a mass and a linear viscous damper i.e. the mechanical element of the energy generating component. Analysis is conducted using the energy conservation principle to reveal a fundamental limit on the performance of any non-linear device compared to that of a *tuned* linear system. The first system employs a bi-stable non-linear spring, termed a snap-through mechanism, which rapidly moves the seismic mass between two stable states. The aim is to steepen the displacement response curve of the mass as a function of time, which results in an increase of the velocity for a given excitation, thus increasing the amount of power harvested. The second non-linear mechanism described in this paper uses a hardening-type stiffness element. The aim of this mechanism is to provide a wider bandwidth over which the power can be harvested so that it can accommodate mistune. The performance of each non-linear system is compared with its respective equivalent linear system.

2 Available power from a non-linear device

In this section, the maximum power harvested by devices that can be modelled as a single degree-of-freedom (SDOF) mechanical system containing linear and non-linear springs is determined. Consider the equation of motion of a base-excited SDOF linear system given by [1, 4]

$$m\ddot{z} + c\dot{z} + kz = -m\ddot{y}, \tag{1}$$

where m is the mass, k is the stiffness and $z = x - y$ is the relative displacement between that of the seismic mass, x, and the housing, y. The amount of energy harvested is represented by the energy dissipated by the dashpot, c, because the conversion of mechanical energy into electrical energy is assumed to have the same effect as mechanical damping. Assuming that $y = Y\cos(\omega t)$ and multiplying both sides of (1) by the relative velocity $\dot{z}$ gives

$$m\ddot{z}\dot{z} + c\dot{z}\dot{z} + kz\dot{z} = m\omega^2 Y(\cos\omega t)\dot{z}. \tag{2}$$

Integrating each term in (2) over one period of the excitation and assuming that the power harvested in

one cycle is the same as the power dissipated by the damper results in

$$P_h = P_{\text{in}}, \tag{3}$$

where $P_h = \frac{\omega}{2\pi}\int_0^{\frac{2\pi}{\omega}} c\dot{z}^2\,dt$ is the harvested power and in this simple model, $P_{\text{in}} = \frac{\omega}{2\pi}\int_0^{\frac{2\pi}{\omega}} m\omega^2 Y(\cos\omega t)\dot{z}\,dt$ is the input power.

Now consider a general non-linear system with the equation of motion given by

$$m\ddot{z} + c\dot{z} + f(z) = -m\ddot{y}, \tag{4}$$

where $f(z)$ is a conservative non-linear spring force. If a similar analysis is conducted and each term in (4) is integrated over a cycle, the result is the same as that in (3). Note that the integrals involving the mass and the stiffness vanish since the net change in the kinetic and potential energies of the system over one period of motion are zero. This occurs for any non-linear mechanism due to the conservative properties of the mass and spring elements.

For the linear system with a given amount of damping, the maximum input power occurs when $\dot{z}$ and y are in phase. This is the case when the system is tuned so that its natural frequency equals the excitation frequency. The power harvested over a cycle for the linear mechanism in this case is given by [7]

$$P_l = \frac{\omega}{2\pi}\int_0^{\frac{2\pi}{\omega}} m\omega^2 Y(\cos\omega t)\dot{z}\,dt = \frac{m\omega^3 YZ}{2}, \tag{5}$$

where Z is the amplitude of the relative displacement between the housing and the seismic mass and the subscript l denotes the linear system. Equation (5) shows that the maximum harvested power depends on the size of the mass, the amplitude of the input displacement, the amplitude of the relative displacement between the seismic mass and the housing and the cube of the excitation frequency. For a device containing a non-linear spring, $\dot{z}$ is not harmonic and so the integral in (5) does not have an analytical solution. However, an upper bound can be found for the power harvested by the non-linear device by noting that

$$P_n \le \frac{\omega}{2\pi}\int_0^{\frac{2\pi}{\omega}} m\omega^2 Y\left|\cos(\omega t)\right||\dot{z}|\,dt, \tag{6}$$

where n denotes the non-linear system. Since $|\cos(\omega t)| \le 1$, the inequality in (6) can be further simplified to

$$P_n \le \frac{m\omega^3 Y}{2\pi}\int_0^{\frac{2\pi}{\omega}} |\dot{z}|\,dt. \tag{7}$$

Because $\dot{z}$ is a periodic function, the integral in (7) can be rewritten as

$$\int_0^{\frac{2\pi}{\omega}} |\dot{z}|\,dt = 4\int_0^{\frac{\pi}{2\omega}} \dot{z}\,dt, \tag{8}$$

which can also be written in terms of the relative displacement z rather than t as

$$4\int_0^{\frac{\pi}{2\omega}} \dot{z}\,dt = 4\int_0^{Z} dz = 4Z. \tag{9}$$

Combining (7), (8) and (9) gives the upper bound for the power harvested by a device containing a non-linear spring

$$P_n \le \frac{2m\omega^3 YZ}{\pi}. \tag{10}$$

For the non-linear case here, $\dot{z}$ can also be expanded as a sum of time harmonics since the motion is assumed to be periodic. However, note that only the first harmonic of the response contributes to the harvested power since the harmonics are orthogonal to each other.

The ratio of the power harvested by a non-linear device to that by a tuned linear device can be found by dividing (10) by (5) to give

$$P_r = \frac{P_n}{P_l} \le \frac{4}{\pi}. \tag{11}$$

However the actual power harvested by a non-linear device depends on the form of the non-linearity $f(z)$. Equation (11) shows that, if optimally tuned, the maximum amount of power harvested by a non-linear mechanism, is $4/\pi$ times larger than the power harvested by the tuned linear system. In the most favourable non-linear system, the displacement response approximates a square wave, so that $\dot{z}$ is non-zero only when $|\cos\omega t| \approx 1$. However, it should be emphasised that the ratio of the power harvested by a device with a non-linear mechanism to that of a linear system may be greater than $4/\pi$ when the linear system is not tuned and hence the non-linear system may be able to cope better with mistune than a linear

system. In this paper, two physically realizable non-linear systems are studied. The first system is a non-linear bi-stable stiffness termed a *snap-through* or a *click* mechanism and the second system is a non-linear system comprising a *hardening* stiffness.

3 Snap-through mechanism

Figure 1 shows a possible arrangement of the mass-spring-damper for the snap-through mechanism. It consists of two linear oblique springs connected to a mass and a damper. Unlike a linear system [1], when the springs are unextended, they are inclined at an angle $\pm\theta$ to the line $x = 0$. Although the springs provide a linear restoring force along their axes, this particular arrangement yields a non-linear restoring force in the x-direction. The purpose of this mechanism is to steepen the gradient of the displacement curve as a function of time so as to approximate a square wave. The snap-through mechanism has been studied by Brennan et al. [10] to model the flight mechanism of an insect; they determined the peak kinetic energy which can be produced using this mechanism and compared it to that for the linear system.

3.1 Static analysis of the oblique springs

This section focuses on a static analysis of the two oblique springs and shows how the arrangement results in a negative stiffness mechanism [10]. Figure 2 shows two inclined springs attached together with an axial force acting on both springs. The total axial component of the spring force F at any displacement x is such that

$$F = 2F_k, \tag{12}$$

where F_k is the axial component of each spring force. The total axial restoring force as a function of x is given by

$$F = 2k_s\left(\sqrt{x^2 + l^2} - l_o\right)\sin\theta, \tag{13}$$

where $\sqrt{x^2 + l^2}$ is the length of the spring, l_o is the original length of the spring and θ is the inclination of the spring with respect to the origin. Referring to Fig. 2,

$$\sin\theta = \frac{x}{\sqrt{x^2 + l^2}}. \tag{14}$$

Substituting this into (13) gives

$$F = 2k_s\left(1 - \frac{l_o}{\sqrt{x^2 + l^2}}\right)x, \tag{15}$$

which can be expressed in dimensionless form as

$$\hat{F} = \left(1 - \frac{1}{\sqrt{\hat{x}^2 + \gamma^2}}\right)\hat{x}, \tag{16}$$

where $\hat{F} = \frac{F}{2k_s l_o}$, $\hat{x} = \frac{x}{l_o}$ and $\gamma = \frac{l}{l_o}$. Figure 3 shows the non-dimensional axial restoring force of the sys-

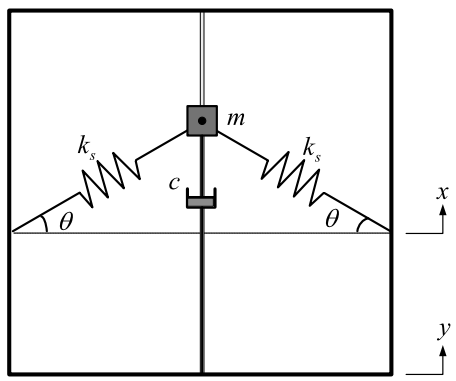

Fig. 1 Arrangement of the mass-spring-damper for the snap-through mechanism

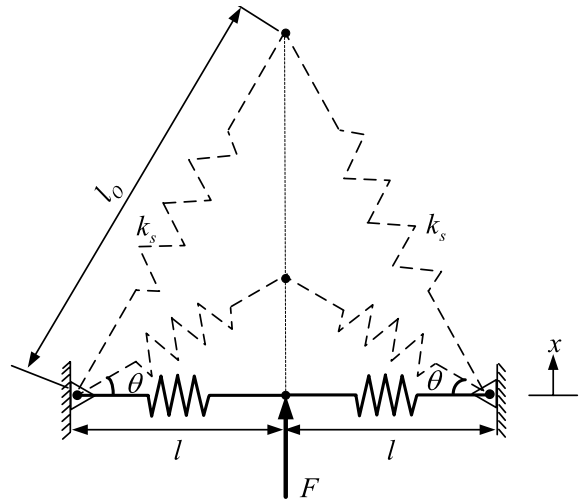

Fig. 2 The force acting on the oblique spring

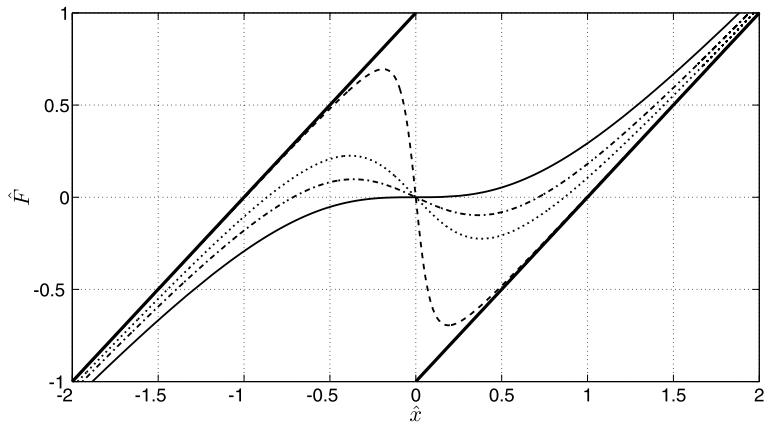

Fig. 3 Non-linear dimensionless restoring force $\hat{F}$ as a function of $\hat{x}$: $\gamma = 0$ (*thick solid line*), $\gamma = 0.1$ $(--)$, $\gamma = 0.5$ $(\cdots)$, $\gamma = 0.7$ $(-\cdot-)$ and $\gamma = 1.0$ (*thin solid line*)

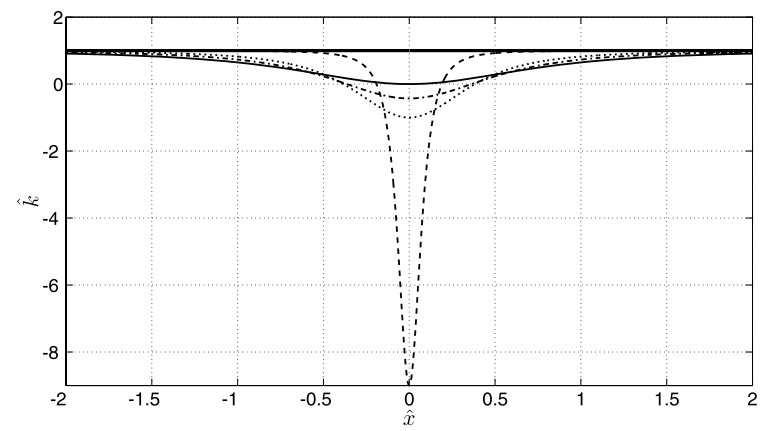

Fig. 4 Dimensionless non-linear stiffness $\hat{k}$ as a function of $\hat{x}$: $\gamma = 0$ (*thick solid line*), $\gamma = 0.1$ $(--)$, $\gamma = 0.5$ $(\cdots)$, $\gamma = 0.7$ $(-\cdot-)$ and $\gamma = 1.0$ (*thin solid line*)

tem as a function of $\hat{x}$ for various γ. The non-dimensional stiffness, $\hat{k} = \frac{d\hat{F}}{d\hat{x}}$ of the system is

$$\hat{k} = 1 - \frac{\gamma^2}{(\hat{x}^2 + \gamma^2)^{\frac{3}{2}}}, \tag{17}$$

where $\hat{k} = \frac{k_n}{2k_s}$ and $k_n = \frac{dF}{dx}$ is the physical stiffness of the system in Fig. 2. The non-dimensional stiffness of the spring is shown in Fig. 4 as a function of $\hat{x}$. It can be seen that it changes from positive to negative and to positive again when $0 < \gamma < 1$.

The total elastic potential energy, E_p is given by

$$E_p = 2\left[\frac{1}{2}k_s\left(\sqrt{x^2 + l^2} - l_o\right)^2\right], \tag{18}$$

which can also be represented in dimensionless form as

$$\hat{E} = \left(\sqrt{\hat{x}^2 + \gamma^2} - 1\right)^2, \tag{19}$$

where $\hat{E} = \frac{E_p}{k_s l_o^2}$. The non-dimensional potential energy is plotted in Fig. 5, which shows that the system has a double-well potential [11, 12]. The equilibrium positions, $\hat{x}_{1,2,3}$ of the system are given by

$$\hat{x}_1 = \sqrt{1 - \gamma^2} \quad \{\text{stable}\}, \tag{20}$$

$$\hat{x}_2 = -\sqrt{1 - \gamma^2} \quad \{\text{stable}\}, \tag{21}$$

$$\hat{x}_3 = 0 \quad \{\text{unstable}\}. \tag{22}$$

If the amplitude of the motion is small, the system will oscillate about one of its stable equilibrium positions depending on the initial conditions. If the amplitude is large, the system starts to oscillate between the two stable equilibrium positions, which can also be described as cross-well motion. The critical static force $\hat{F}_C = \frac{d\hat{F}}{d\hat{x}}$ that the system can withstand before snap-through occurs is given by

$$\hat{F}_C = \left(1 - \gamma^{\frac{2}{3}}\right)^{\frac{3}{2}}. \tag{23}$$

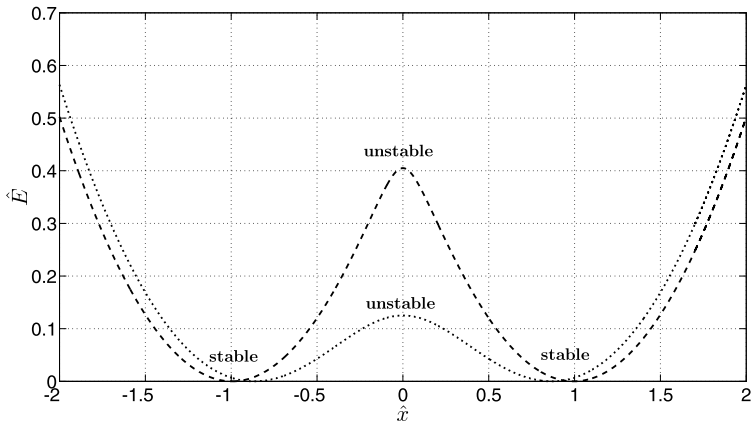

Fig. 5 Dimensionless elastic potential energy $\hat{E}$ of the springs as a function of position $\hat{x}$: $\gamma = 0.1$ (−−) and $\gamma = 0.5$ (···)

This shows that the smaller the value of γ, the larger the force needed to snap the spring from one equilibrium position to another. Substituting $\hat{F}_C$ into (16) and solving for $\hat{x}$ gives the position at which the snap-through occurs

$$\hat{x}_C = \gamma^{\frac{2}{3}}\sqrt{1-\gamma^{\frac{2}{3}}}. \tag{24}$$

3.2 Numerical simulation of the power harvested

The power harvested by the device containing either linear or snap-through mechanisms as a function of frequency is discussed in this section. A numerical simulation is conducted to compare the performance of both systems. The equation of motion of a linear system described in (1) can be written in dimensionless form as

$$u'' + 2\zeta u' + u = \Omega^2 \hat{Y}\cos(\Omega\tau), \tag{25}$$

where $u = \frac{z}{l_o}$, $\omega_n^2 = \frac{k}{m}$, $\tau = \omega_n t$, $\Omega = \frac{\omega}{\omega_n}$, $\zeta = \frac{c}{2m\omega_n}$, $\hat{Y} = \frac{Y}{l_o}$, $(\bullet)' = \frac{d}{d\tau}$ and $(\bullet)'' = \frac{d^2}{d\tau^2}$.

The equation of motion of the snap-through mechanism given by (4) can also be written in dimensionless form where the non-linear stiffness force $f(z)$ of the form given in (16) is used to give

$$u'' + 2\zeta u' + \left(1 - \frac{1}{\sqrt{u^2+\gamma^2}}\right)u = \Omega^2 \hat{Y}\cos(\Omega\tau), \tag{26}$$

where $0 < \gamma < 1$. Here $\Omega = \frac{\omega}{\omega_n}$ where $\omega_n = \sqrt{\frac{2k_s}{m}}$ is the natural frequency of small amplitude vibrations about a stable equilibrium position. The non-dimensional power harvested by the device for both linear and snap-through mechanisms is obtained numerically using the equivalent non-dimensional expression for power dissipated by the damper, P_h as described in (3)

$$\hat{P} = \frac{\Omega\zeta}{\pi}\int_0^{\frac{2\pi}{\Omega}} (u')^2\, d\tau, \tag{27}$$

where $\hat{P} = \frac{P}{m\omega_n^3 l_o^2}$. Equation (26) is solved numerically using the 4th order Runge–Kutta method and the power harvested is calculated using (27).

Figure 6 shows the power harvested for the linear system and the snap-through mechanism for different values of γ. It should be noted that the system parameters are fixed, rather than being optimised to produce maximum harvested power at any frequency Ω. The main objective of the simulation is to investigate the general trend of the power harvested by the device with the snap-through mechanism and to compare it with that for the linear mechanism. It can be seen in Fig. 6 that there is a sudden increase in the power harvested with the snap-through mechanism when $\gamma = 0.1$ and $\Omega \approx 0.2$. Equation (23) shows that, the smaller the value of γ, the larger the force needed to move the mass from one equilibrium position to the other. Thus when $\gamma = 0.1$ and $\Omega = 0.1$, the mass just oscillates about one of its stable equilibrium positions resulting in a small amount of power being harvested. When Ω is increased to about 0.2, the excitation is large enough to oscillate the mass between the two stable equilibrium positions, which reflects the sudden increase in the harvested power. This is not the case for the system with $\gamma = 0.5$ since the input is large enough to throw the mass between the two stable equilibrium positions even when $\Omega = 0.1$. It can also be seen in

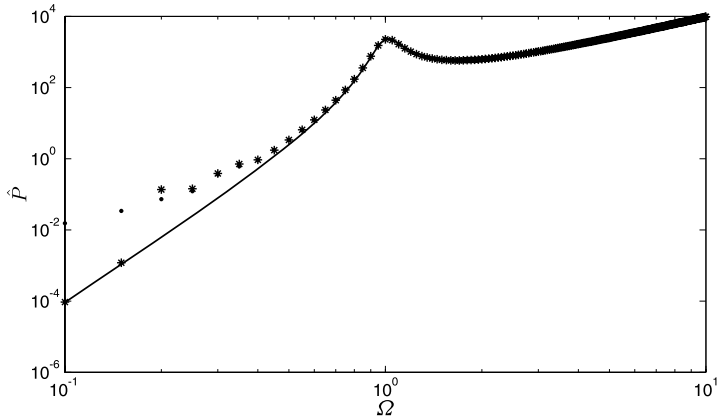

Fig. 6 Power harvested in the damper when $\zeta = 0.1$ and $\hat{Y} = 30$: linear mechanism (—), snap-through mechanism $\gamma = 0.1$ ($*$) and snap-through mechanism $\gamma = 0.5$ ($\bullet$)

Fig. 6 that the snap-through mechanism outperforms the linear mechanism at low frequencies. The snap-through mechanism starts to behave like a linear system at about $\Omega \approx 0.6$ due to the large response. At low frequencies, the rate at which the normalised power increases with frequency is 60 dB per decade for the linear case but only about 30 dB per decade for the non-linear case. Thus considerably more power can be harvested from the non-linear system if Ω is much less than unity.

3.3 Practical constraints

Equation (11) suggests that the maximum amount of power harvested by a non-linear mechanism can be at most $4/\pi$ greater than the *tuned* linear mechanism assuming that the output displacement, for a given sinusoidal input, is a square wave. However, Fig. 6 shows that the power harvested by the snap-through mechanism is much greater than that harvested by the linear system at low frequencies. This is because the linear system is tuned to only one excitation frequency and the power harvested drops off rapidly for excitation away from the natural frequency of the device. The ideal response of the snap-through mechanism is a square wave for the displacement. However, the response has to satisfy the equation of motion given in (26), thus an approximation to the square wave is produced, instead. This approximation becomes worse at high frequencies. To produce a good approximation to a square wave, the rise time τ_r (time to travel from $z = 0$ to $z = Z$) has to be much shorter than a quarter of a period i.e. $\tau_r \ll T/4$, where $T = 2\pi/\Omega$ is the period of oscillation. For a given physical system, τ_r is further limited by the presence of the mass and the damping. As the frequency increases, the system is unable to produce a square-wave-like response since the period becomes shorter and the condition $\tau_r \ll T/4$ can no longer be achieved. As a result, an approximately sinusoidal response is produced at high frequencies rather than a square wave, which results in a similar amount of power harvested as the linear device. As shown in Fig. 6, the power harvested at low frequencies by the linear system rolls off at a higher rate than the system with the snap-through mechanism. Thus a potential benefit of this mechanism is that it can accommodate mistune better. Also the figure shows that the real benefit of the snap-through mechanism is by having a system with a much higher natural frequency compared to the excitation frequency.

4 Hardening mechanism

In Sect. 3, it was shown that it is not possible for a mechanical system to produce a perfect square wave. Thus the performance ratio of $4/\pi$ between a non-linear and a linear system may not be achievable. In this section, another type of non-linear system termed a hardening mechanism is considered. This type of non-linear system is used to provide a greater bandwidth over which the power can be harvested by shifting the resonance frequency to a higher frequency. Thus the discussion on this hardening mechanism mainly focuses on the determination of the bandwidth. While such a mechanism can be obtained from a snap-through mechanism by setting $\gamma > 1$ into (26), the equation of motion used here is

$$m\ddot{z} + c\dot{z} + k_l z\left(1 + \frac{k_n}{k_l} z^2\right) = -m\ddot{y}. \tag{28}$$

The system consists of a mass connected in series with a parallel combination of a damper and a non-linear spring whose spring force is of the form $k_l x + k_n x^3$. The system is base-excited with $k_n > 0$ denoting a hardening system. Equation (28) can be expressed in non-dimensional form as

$$u'' + 2\zeta u' + u + \alpha u^3 = \hat{Y}_e \cos(\Omega\tau). \tag{29}$$

In this case $\omega_n = \sqrt{\frac{k_l}{m}}$, $\Omega = \frac{\omega}{\omega_n}$, $u = \frac{z}{X_o}$, $X_o = \frac{mg}{k_l}|_{k_n=0,\omega=0}$, $\alpha = \frac{k_n X_o^2}{k_l}$, $\hat{Y}_e = \frac{\Omega^2 Y}{X_o} = \frac{\omega^2 Y}{g}$ and g is the acceleration due to gravity.

It is assumed that higher order harmonics are negligible and that the steady-state solution of (29) is of the form

$$u = U\cos(\Omega\tau + \phi), \tag{30}$$

where U is the amplitude and ϕ is the phase of the response. Solving (29), using the Harmonic Balance method [14], yields

$$\left(\frac{3}{4}\alpha U^2 + 1 - \Omega^2\right)^2 + (2\zeta\Omega)^2 = \left(\frac{\hat{Y}_e}{U}\right)^2. \tag{31}$$

Solving (31) for positive Ω gives the frequency-amplitude relationship for light damping (such that $\zeta^2 \ll 1$) as

$$\Omega_a \approx \left[1 + \frac{3}{4}\alpha U^2 - \frac{(\hat{Y}_e^2 - 3\alpha\zeta^2 U^4 - 4\zeta^2 U^2)^{\frac{1}{2}}}{U}\right]^{\frac{1}{2}}, \tag{32}$$

$$\Omega_b \approx \left[1 + \frac{3}{4}\alpha U^2 + \frac{(\hat{Y}_e^2 - 3\alpha\zeta^2 U^4 - 4\zeta^2 U^2)^{\frac{1}{2}}}{U}\right]^{\frac{1}{2}}, \tag{33}$$

where (32) gives the resonant response (steady-state response with a larger amplitude at a given frequency) and (33) gives the non-resonant response (steady-state response with a smaller amplitude) of the system, in the region where multiple stable solutions exist.

4.1 Frequency-response curves

Figure 7 shows a typical frequency-response curve (FRC) for a hardening system plotted using equations (32) and (33) for arbitrary system parameters. The solid line represents the stable steady-state solution and the dashed line denotes the unstable steady-state solution. The maximum response is depicted by U_m and the frequency when the maximum response occurs is given by Ω_m. U_2 and Ω_2 represents the jump-down amplitude and frequency, respectively. The backbone curve of the system is the response for undamped free vibration of the system, i.e. $\hat{Y}_e = \zeta = 0$. The amplitude of the half-power point is given by U_1 while the frequencies of the half-power points are respectively represented by Ω_1 (on the curve plotted using (32)) and $\Omega_{1'}$ (on the backbone curve). An approximation for the maximum amplitude, U_m, and

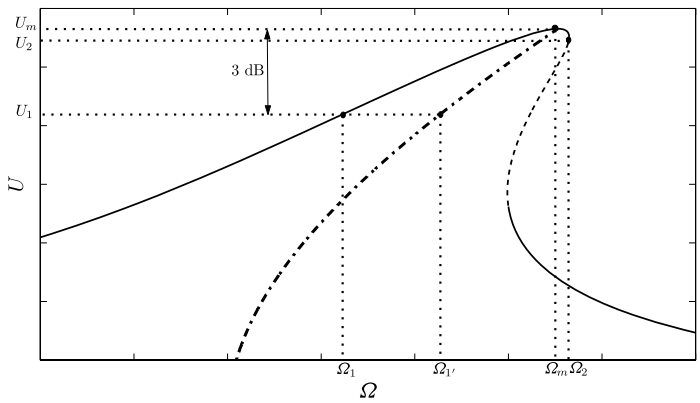

Fig. 7 Typical frequency-response curve for a hardening system; U_m and Ω_m are the maximum response and frequency at which the maximum response occurs respectively, U_2 and Ω_2 are the jump-down amplitude and the jump-down frequency respectively, U_1 and Ω_1 are the half-power point amplitude and frequency respectively, and $\Omega_{1'}$ is the half-power point frequency on the backbone curve ($- \cdot -$). The solid line represents the *stable* branch and the dashed line represents the *unstable* branch

frequency, Ω_m, of the system can be found using the backbone curve, which is given by

$$\Omega^2 = 1 + \frac{3}{4}\alpha U^2, \tag{34}$$

which reduces to the resonance frequency of the linear system, $\Omega = 1$, when $\alpha = 0$. The amplitude at the maximum response, U_m can be determined by setting the internal radicand in (32) to zero, to give

$$\hat{Y}_e^2 - 3\alpha\zeta^2 U_m^4 - 4\zeta^2 U_m^2 = 0. \tag{35}$$

Solving (35) gives the maximum response to be

$$U_m = \left[\frac{2}{3\alpha}(\mu - 1)\right]^{\frac{1}{2}}, \tag{36}$$

where $\mu = (1 + \frac{3\alpha}{4\zeta^2}\hat{Y}_e^2)^{\frac{1}{2}}$. Substituting (36) into (32) and rearranging gives the frequency at which the maximum response occurs

$$\Omega_m = \left[\frac{1}{2}(1 + \mu)\right]^{\frac{1}{2}}. \tag{37}$$

These two equations relating the maximum response, U_m, and the frequency at which the maximum response occurs, Ω_m, are used in the next section to determine the bandwidth of the hardening system.

4.2 Bandwidth of the hardening system

Referring to Fig. 7, the bandwidth of the hardening system, $\Delta\Omega_h$, is defined as

$$\Delta\Omega_h = (\Omega_2 - \Omega_m) + (\Omega_m - \Omega_1). \tag{38}$$

If $\zeta^2 \ll 1$ and $\zeta^2 \ll \alpha$, the jump-down frequency, Ω_2 is approximately equal to the maximum response frequency, Ω_m, and (38) reduces to

$$\Delta\Omega_h \approx \Omega_m - \Omega_1. \tag{39}$$

The half-power point amplitude U_1 is obtained by dividing the maximum response, U_m in (36) by $\sqrt{2}$ to yield

$$U_1 = \left[\frac{1}{3\alpha}(\mu - 1)\right]^{\frac{1}{2}}. \tag{40}$$

Substituting U_1 into (32) gives the half-power point frequency Ω_1 such that

$$\Omega_1 = \left[\frac{3}{4} + \frac{1}{4}\mu - \zeta(1 + 3\mu)^{\frac{1}{2}}\right]^{\frac{1}{2}}. \tag{41}$$

The approximate expression for the bandwidth of the hardening system is thus given by substituting (37) and (41) into (39) to give

$$\Delta\Omega_h \approx \frac{1}{2}\left[\sqrt{2}(1 + \mu)^{\frac{1}{2}} - \left(3 + \mu - 4\zeta(1 + 3\mu)^{\frac{1}{2}}\right)^{\frac{1}{2}}\right]. \tag{42}$$

It can be seen that the bandwidth of the hardening system is dependent on the damping ratio ζ, the non-linearity α and the input acceleration $\hat{Y}_e$. Given that the bandwidth of the linear system is equal to 2ζ [13], Fig. 8 shows the plot of bandwidths for linear and hardening systems obtained using (42). The bandwidth of the linear system increases linearly with the damping ratio, ζ. For a given ζ such that $\zeta \ll 1$,

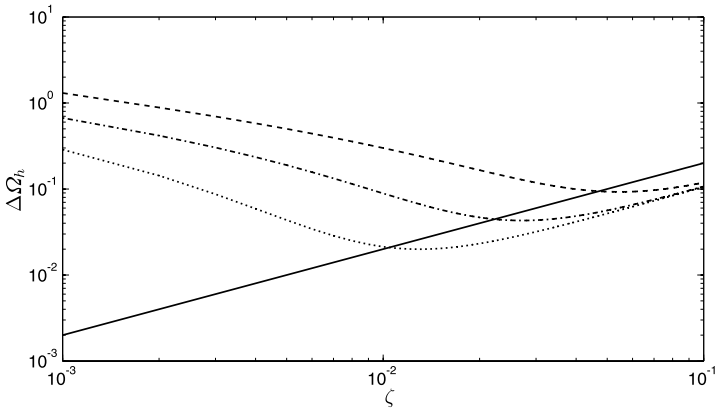

Fig. 8 Bandwidth of a linear and hardening systems (42) with $\hat{Y}_e = 0.5$: linear (—), hardening ($\cdots$ $\alpha = 0.0001$), hardening ($-\cdot-$ $\alpha = 0.001$) and hardening ($--$ $\alpha = 0.01$)

and $\hat{Y}_e$, the bandwidth of the hardening system increases with the degree of non-linearity, α. The differences for large ζ are due to the approximation $\Omega_m = \Omega_2$.

4.3 Approximation for the bandwidth based on the backbone curve

The approximate expression for the bandwidth given in (42) is fairly complicated. Thus an approximate and reasonably accurate simple expression for the bandwidth is sought. To do this, it is assumed that the frequency of the half-power point $\Omega_1 \approx \Omega_{1'}$, where $\Omega_{1'}$ is the half-power point frequency on the backbone curve as illustrated in Fig. 7. This is a reasonable assumption provided that $\frac{3\alpha\hat{Y}_e^2}{4\zeta^2} \gg 1$. Using the expression for the backbone curve in (34), the frequency at which the half-power point amplitude occurs on the backbone curve is given by

$$\Omega_{1'}^2 = 1 + \frac{3}{4}\alpha\left(\frac{U_m}{\sqrt{2}}\right)^2. \tag{43}$$

Substituting the expression for U_m from (36) into (43) gives

$$\Omega_{1'} = \frac{1}{2}(3+\mu)^{\frac{1}{2}}. \tag{44}$$

The approximate bandwidth of the hardening system $\Delta\Omega_h'$ determined using this method is simply given by

$$\Delta\Omega_h' \approx \Omega_m - \Omega_{1'}, \tag{45}$$

$$\Delta\Omega_h' \approx \frac{1}{2}\left[\sqrt{2}(1+\mu)^{\frac{1}{2}} - (3+\mu)^{\frac{1}{2}}\right]. \tag{46}$$

4.4 Practical constraints

One of the main differences between a linear and a non-linear system is that a non-linear system can produce multiple stable steady-state solutions which are dependent on a set of initial conditions. A linear system however always produces a unique stable solution for all initial conditions.

In this section, the analytical and numerical solutions of the hardening system are studied. Figure 9 shows the FRCs for different values of non-linearity, α. The numerical solutions are found by direct integration of the equation of motion and the steady-state solution is compared with the approximate solution obtained using the harmonic balance method. It can be seen that the analytical solutions agree quite well with the numerical results, for the parameters chosen.

In the frequency range where multiple stable solutions exist, different initial conditions give different steady-state solutions. If certain initial conditions are applied to the system, the steady-state solution converges to the lower of the two possible values. To study the effect of the initial conditions on the steady-state response of the hardening system, the basins of attraction are produced for each case shown in Fig. 9. The basin of attraction is shown in such a way that the

- White region gives the initial conditions that result in the response being on the resonant branch (larger amplitude).
- Dark region gives the initial conditions that result in the response being on the non-resonant branch (smaller-amplitude).

For the case where $\alpha = 0.001$ (moderate non-linearity), at a frequency reasonably far from the jump-down frequency ($\Omega = 1.1$), there is a fairly large set of initial conditions for which the steady-state solution is on the resonant branch as shown in Fig. 10(a). As the frequency gets closer to the jump-down frequency, the set of initial conditions for which the steady-state solution is on the resonant branch decreases as shown in Figs. 10(b) and 10(c) for $\Omega = 1.15$ and $\Omega = 1.16$, respectively. For a larger non-linearity, $\alpha = 0.01$, the change in the basin area for the resonant branch is more dramatic especially in the region close to the jump-down point as shown by Fig. 11.

Assuming that it is possible to obtain a numerical solution using suitable initial conditions which converges to the resonant branch, the power harvested in the damper can also be calculated numerically using equation (27). In this case, $\hat{P} = \frac{P}{m\omega_n^3 X_o^2}$. The non-dimensional power harvested for the linear and hardening systems is plotted in Fig. 12 for $\zeta = 0.01$, $\hat{Y}_e = 0.5$ and for various α. Even though the maximum displacement U_m decreases with the non-linearity α as shown in Fig. 9, the maximum normalised power harvested is almost the same for all cases but occurs at a different frequency. In practice, however, it may not be possible to achieve this because of the initial conditions needed. The favourable combination of these is quite limited, as illustrated by the domains of the periodic attractors.

To study the effect of the non-linearity, α on the maximum power harvested, it is necessary to examine

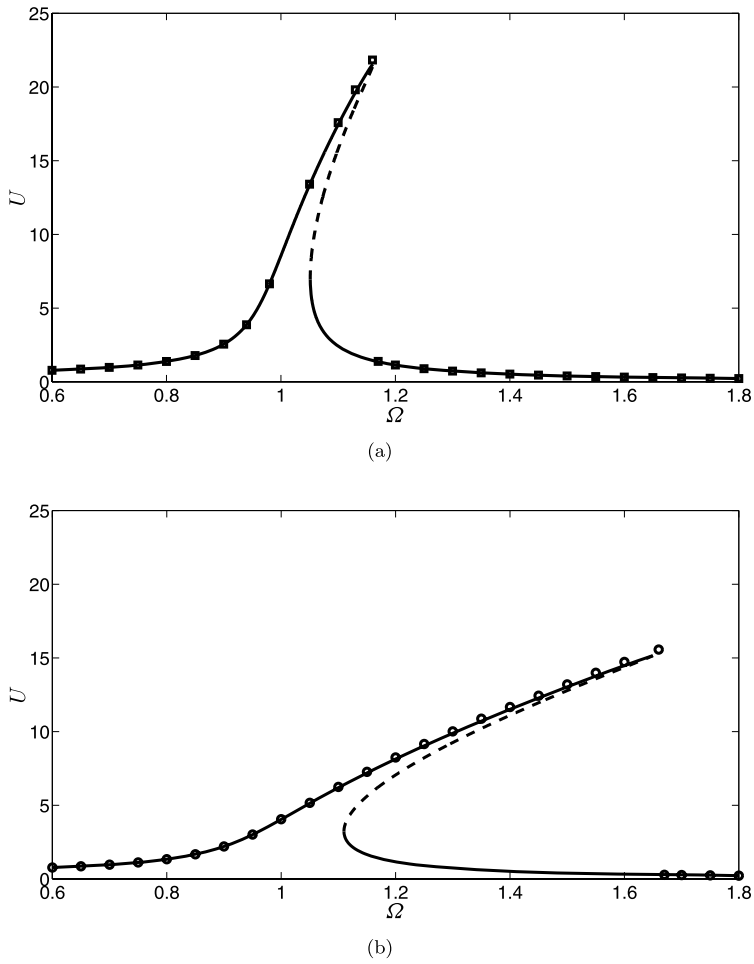

Fig. 9 Frequency-response curve for the hardening system with $\zeta = 0.01$ and $\hat{Y}_e = 0.5$ for (**a**) $\alpha = 0.001$ and (**b**) $\alpha = 0.01$: analytical solution (*solid lines*, *dashed lines*) and numerical solution (□, ○)

the FRC for the velocity response rather than displacement since power is a function of velocity. The amplitude of the velocity response is given by

$$|u'| = \Omega U. \tag{47}$$

The amplitude of the velocity, $|u'|_m$ at the jump-down frequency, which is approximately the maximum velocity, is given by substituting U_m from (36) for U in (47), which simplifies to give

$$|u'|_m = \frac{\hat{Y}_e}{2\zeta}. \tag{48}$$

Thus because the maximum velocity is independent of the non-linearity, α, the maximum power harvested for different values of α is also independent of the non-linearity.

5 Conclusions

In this paper two non-linear mechanisms for energy harvesting devices have been investigated. The first one was a non-linear bistable single degree-of-freedom mass-spring-damper system, which results in a negative stiffness that steepens the gradient of the displacement response as a function of time and hence increases the maximum velocity. Static analysis was conducted to show how the spring arrangement can be used to produce a region with negative stiffness. This study also revealed that the amount of power harvested by a non-linear device is at most $4/\pi$ greater than that of the *tuned* linear device provided the device produces a square wave output for given sinusoidal input. The snap-through mechanism is unable to produce a square-wave-like response that satisfies all operating conditions. However, the mechanism of-

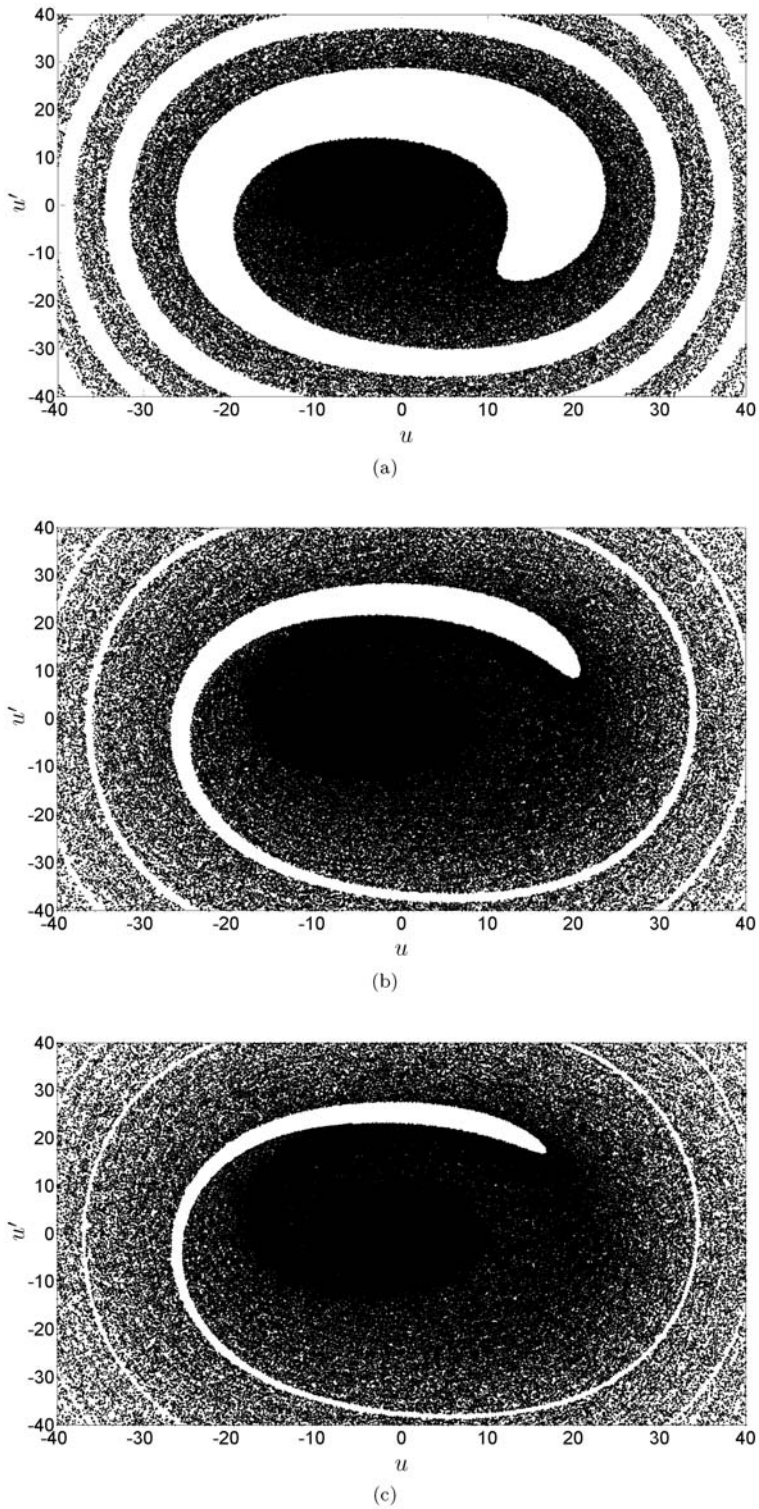

Fig. 10 Basin of attraction for the hardening system with $\alpha = 0.001$, $\zeta = 0.01$ and $\hat{Y}_e = 0.5$ corresponding to the FRC in Fig. 9(a) when (**a**) $\Omega = 1.1$, (**b**) $\Omega = 1.15$ and (**c**) $\Omega = 1.16$ (jump-down frequency, $\Omega_m \approx 1.170$)

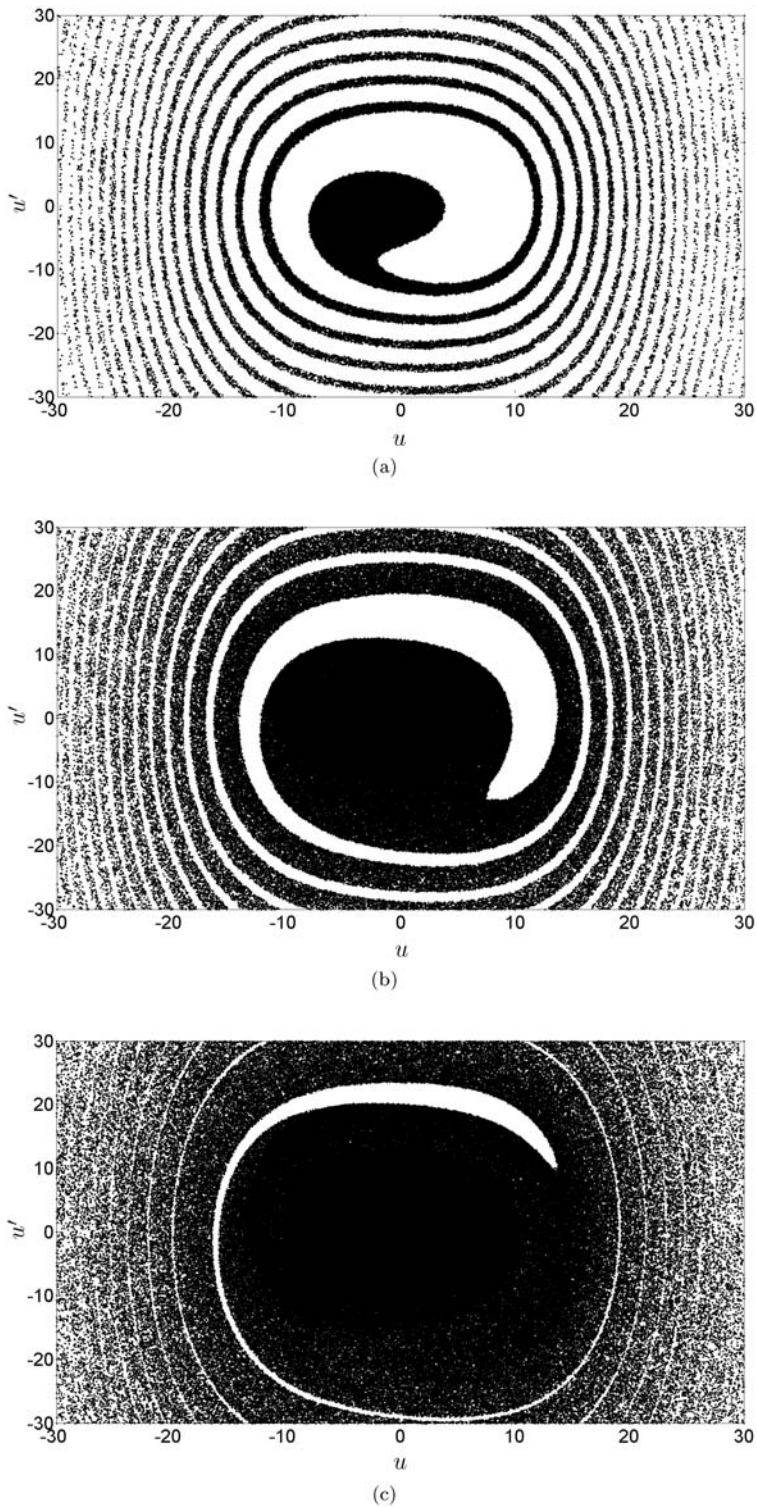

Fig. 11 Basin of attraction for the hardening system with $\alpha = 0.01$, $\zeta = 0.01$ and $\hat{Y}_e = 0.5$ corresponding to the FRC in Fig. 9(b) when (**a**) $\Omega = 1.2$, (**b**) $\Omega = 1.4$ and (**c**) $\Omega = 1.6$ (jump-down frequency, $\Omega_m \approx 1.665$)

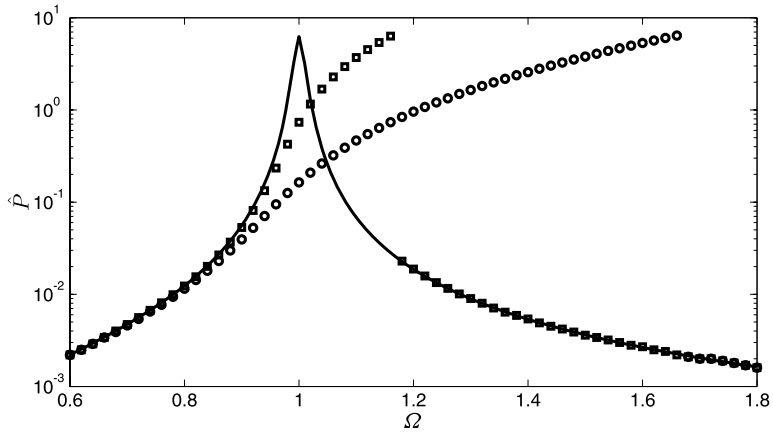

Fig. 12 Numerical solution for non-dimensional power harvested with $\zeta = 0.01$ and $\hat{Y} = 0.5$: Linear system (*solid line*) and, hardening systems $\alpha = 0.001$ (□) and $\alpha = 0.01$ (○)

fers better performance than the linear mechanism at low frequencies and also has the potential to cope with mistune. The second mechanism is a non-linear mechanism with a hardening stiffness. The harmonic balance method was used to solve the equation of motion and obtain the frequency–response relationship. The analysis shows that the bandwidth of the hardening system depends on the damping ratio, the non-linearity and the input acceleration. Although the harmonic balance solution using just one harmonic matched the numerical simulation results for the range of parameters studied, the basins of attraction revealed that it may not be easily achievable in practice. Ideally, the maximum amount of power harvested by a system with a hardening stiffness is the same as the maximum power harvested by a linear system, irrespective of the degree of the non-linearity, although this may occur at a different frequency depending on the degree of non-linearity.

Acknowledgements Ramlan would like to acknowledge the financial support from the Government of Malaysia and the Universiti Teknikal Malaysia Melaka (UTeM) for the Bumiputera Academic Training Scheme (SLAB) scholarship award. Professors Brennan and Kovacic would like to acknowledge the support received from the Royal Society, UK, International Joint Project 'Using nonlinearity to improve the performance of vibrating systems'.

References

1. Williams, C.B., Yates, R.B.: Analysis of a micro-electric generator for microsystems. Sens. Actuators A **52**, 8–11 (1996)
2. Beeby, S.P., Tudor, M.J., White, N.M.: Energy harvesting vibration sources for microsystems applications. Meas. Sci. Technol. **17**, R175–R195 (2006)
3. Sari, I., Balkan, T., Kulah, H.: A wideband electromagnetic micro power generator for wireless microsystems. In: The 14th International Conference on Solid-State Sensors, Actuators and Microsystems, Lyon, France, pp. 275–278 (2007)
4. Stephen, N.G.: On energy harvesting from ambient vibration. J. Sound Vib. **293**, 409–425 (2006)
5. Kulah, H., Najafi, K.: An electromagnetic micro power generator for low-frequency environmental vibrations. In: 17th IEEE International Conference on Micro Electro Mechanical Systems (MEMS), pp. 237–240 (2004)
6. Lee, D., Carman, G., Murphy, D., Schulenburg, C.: Novel micro vibration energy harvesting device using frequency up conversion. In: The 14th International Conference on Solid-State Sensors, Actuators and Microsystems, Lyon, France, pp. 871–874 (2007)
7. Mitcheson, P.D., Green, T.C., Yeatman, E.M., Holmes, A.S.: Architectures for vibration-driven micropower generators. J. Microelectromech. Syst. **13**, 429–440 (2004)
8. Buren, T.V., Mitcheson, P.D., Green, T.C., Yeatman, E.M., Holmes, A.S., Troster, G.: Optimization of inertial micropower generators for human walking motion. IEEE Sens. J. **6**, 28–38 (2006)
9. Burrow, S., Clare, L.: A resonant generator with non-linear compliance for energy harvesting in high vibrational environments. In: IEEE International Conference on Electric Machines & Drives Conference, Antalya, Turkey, pp. 715–720 (2007)
10. Brennan, M., Elliott, S., Bonello, P., Vincent, J.: The "click" mechanism in dipteran flight: if it exists, then what effect does it have? J. Theor. Biol. **224**, 205–213 (2003)
11. Holmes, P.: A nonlinear oscillator with a strange attractor. Philos. Trans. R. Soc. Lond. Ser. A, Math. Phys. Sci. **292**, 419–418 (1979)
12. Moon, F.C.: Chaotic Vibrations: An Introduction for Applied Scientist and Engineers. Wiley, New York (1978)
13. Rao, S.S.: Mechanical Vibrations. Prentice Hall, New Jersey (2004)
14. Tse, F.S., Morse, I.E., Hinkle, R.T.: Mechanical Vibrations: Theory and Applications. Allyn and Bacon, Boston (1978)